THE ASTROPHYSICAL JOURNAL, 493:247–259, 1998 January 20

A NEW LOOK AT CARBON ABUNDANCES IN PLANETARY NEBULAE. III. DDDM1, IC 3568, IC 4593, NGC 6210, NGC 6720, NGC 6826, AND NGC 7009

K. B. KWITTER[1]
Department of Astronomy, Williams College, Williamstown, MA 01267; kkwitter@williams.edu

AND

R. B. C. HENRY[1]
Department of Physics and Astronomy, Room 131, Nielsen Hall, University of Oklahoma, Norman, OK 73019-0225; henry@phyast.nhn.uoknor.edu

Received 1997 January 9; accepted 1997 August 27

ABSTRACT

This paper is the third in a series reporting on a study of carbon abundances in a carefully chosen sample of planetary nebulae representing a large range in progenitor mass and metallicity. We make use of the *IUE* Final Archive database containing consistently reduced spectra to measure line strengths of C III] λ1909 along with numerous other UV lines for the planetary nebulae DDDM1, IC 3568, IC 4593, NGC 6210, NGC 6720, NGC 6826, and NGC 7009. We combine the *IUE* data with line strengths from optical spectra obtained specifically to match the *IUE* slit positions as closely as possible, in order to determine values for the abundance ratios He/H, O/H, C/O, N/O, and Ne/O. The ratio of C III] λ1909/C II λ4267 is found to be effective for merging UV and optical spectra when He II λ1640/λ4686 is unavailable. Our abundance determination method includes a five-level program whose results are fine-tuned by corrections derived from detailed photoionization models constrained by the same set of emission lines. All objects appear to have subsolar levels of O/H, and all but one show N/O levels above solar. In addition, the seven planetary nebulae span a broad range in C/O values. We infer that many of our objects are matter-bounded, and thus the standard ionization correction factor for N/O may be inappropriate for these PNs. Finally, we estimate C/O using both collisionally excited and recombination lines associated with C^{+2} and find the well-established result that abundances from recombination lines usually exceed those from collisionally excited lines by several times.

Subject headings: ISM: abundances — planetary nebulae: general — stars: evolution — ultraviolet: ISM

1. INTRODUCTION

We report further on a project whose aim is to determine the stellar yield of carbon as a function of stellar mass and metallicity for intermediate-mass stars, those in the mass range $0.8 < M < 8\ M_{\odot}$. These stars are predicted to produce as much as 50% of the carbon in the Galaxy (Henry, Kwitter, & Buell 1998). In our general study, measured line intensities are used in five-level atom and photoionization model calculations to determine the abundance ratio of C/O in particular, but also of He/H, O/H, N/O, and Ne/O for 22 planetary nebulae (PNs) selected to represent a broad range in progenitor mass and metallicity. Ultimately, we will use our abundance results as constraints for our own stellar evolution models in order to derive the stellar yield of carbon as a function of these two parameters. We have measured *IUE* spectra of PNs containing strong, collisionally excited carbon emission lines, spectra which have been rereduced in a systematic way and are now in the Final Archive. In two earlier papers, the UV data were joined with optical data from the literature; beginning with this paper, we use new optical data acquired specifically for this project.

In our first paper (Henry, Kwitter, & Howard 1996, hereafter Paper I), we listed our sample objects, described our project in detail, and presented results for the first four PNs. In our second paper (Kwitter & Henry 1996), we reported on five additional PNs. In the current paper, we describe our analysis of seven more objects: DDDM1, IC 3568, IC 4593, NGC 6210, NGC 6720, NGC 6826, and NGC 7009. Future papers will report on the remaining six objects, as well as present and discuss stellar model predictions of carbon yields for intermediate-mass stars. In § 2, we describe the data used in the analysis of these seven objects; the abundance calculations and results are presented in § 3; and a summary is contained in § 4. More detailed discussion of the project and procedures can be found in Paper I.

2. DATA

2.1. *Optical Observations*

The optical data were obtained at KPNO during 1996 May 18–21 with the 2.1 m Goldcam CCD spectrometer. The chip is a Ford 3 K × 1 K CCD with 15 μm pixels. We used a 5″ wide slit that extended 285″ in the E-W direction, with a spatial scale of 0.″78 pixel^{-1}. Using a combination of two gratings, we obtained spectral coverage from 3700 to 9600 Å with overlapping coverage from ~5750 to 6750 Å. Wavelength dispersion was 1.5 Å pixel^{-1} (~8 Å FWHM resolution) for the blue and 1.9 Å pixel^{-1} (~10 Å FWHM resolution) for the red. The usual bias and twilight flat-field frames were obtained each night, along with HeNeAr comparison spectra for wavelength calibration and standard star spectra for sensitivity calibration. Since the chip is thinned, it produces interference fringes visible in the red. In our red spectra, the fringes appear at the ±1% level at ~7500 Å and increase in amplitude with increasing wavelength: ±1.5% at 8000 Å, ±4.5% at 8500 Å, and ±6% at 9000 Å. However, even at their worst, i.e., at ~9500 Å, the

[1] Visiting Astronomer, Kitt Peak National Observatory, National Optical Astronomy Observatories, which is operated by the Association of Universities for Research in Astronomy (AURA), Inc., under cooperative agreement with the National Science Foundation.

TABLE 1

FINAL ARCHIVE SPECTRA

Object	SWP	Exposure Time (s)
DDDM1	23872	08100
	39590	06720
	23840	03600
IC 3568	05432	01200
	47015	00900
	47016	00900
IC 4593	33382	01200
	33383	02400
NGC 7009a	45043	00600
NGC 7009b	45047	01800
NGC 7009c	45619	22500
NGC 7009d	45045	01800
NGC 6720a	41639	04800
NGC 6720b	07231	05400
NGC 6210	14650	02100
	14651	02100
NGC 6826a	25255	00480
NGC 6826b	14615	02400
	14616	01200
NGC 6826c	25254	00600

longest wavelength we measure, the fringe amplitude reaches only about $\pm 7\%$. Internal quartz flats were taken at the position of each object both before and after the object integrations in anticipation of removing the fringes during data reduction. It turned out, however, that more noise was introduced in this process than was removed; we therefore decided to leave the fringes untouched, and to accept this additional uncertainty in our line intensities longward of ~ 7500 Å.

The original images were reduced in the standard fashion using IRAF.[2] Using tasks in the KPNOSLIT package, these two-dimensional spectra were converted to one dimension by extracting a specific section along the slit. The location of the extracted section was chosen to maximize the overlap with the *IUE* slit.

2.2. *UV Data*

All UV spectra used for this project have been obtained from the *IUE* Final Archive. Spectra in the Final Archive have been systematically and uniformly reprocessed by *IUE* staff using the NEWSIPS algorithms, and they represent the best available calibration of these data. The spectra we use are all short-wavelength (SWP), low-dispersion, and large-aperture ($21\farcs7 \times 9\farcs1$) spectra. Table 1 lists the spectra that were measured for each of the seven program objects considered here, along with their integration times.

2.3. *Slit Positions*

The placement of the Goldcam slit in each target PN was chosen to coincide as closely as possible with the location of the best *IUE* observations for which detailed positional information was available. Since the position angle of the Goldcam slit is fixed at 90° while the *IUE* slit position angle is not, the quality of the overlap varies and will be described below for each object. We also note that, because of the 2:1 relative slit widths, the largest possible overlap of the Goldcam slit onto the *IUE* slit is $\sim 50\%$.

For each object, we now describe the *IUE* and optical observations with regard to slit position. In general, our optical N-S offsets from the central star or the center of the nebula match the *IUE* N-S offsets; the E-W component (if any) of the *IUE* offset is matched in the extraction process that creates a one-dimensional spectrum from the appropriate portion of the two-dimensional spectrum.

DDDM1.—All three of the *IUE* spectra were centered on the central star, as were our optical spectra. The position angles of the *IUE* spectra are very similar: 349°, 346°, and 345°. Since the optical diameter of DDDM1 is $0\farcs6$ (Acker et al. 1992), the entire nebula was included in both *IUE* and optical observations, rendering moot the issue of overlap.

IC 4593.—Both *IUE* spectra were centered 7″ S of the center of light (which we are assuming coincides with the center of the nebula), at a position angle of 120°. Our slit was centered 3″ S of the nebula center, which we judge to be fair overlap.

IC 3568.—All three *IUE* spectra were centered on the central star at position angles of $13\fdg6$, 108°, and 328°. Our slit was centered 4″ N of the central star, and we judge the overlap to be reasonably good.

NGC 7009.—Positions for the four *IUE* spectra we used for NGC 7009 were kindly provided by F. Bruhweiler (1996, private communication). Position *a* was located $9\farcs3$ S, 9″ E of the central star, at a position angle of 139°. For position *b*, the *IUE* slit was $9\farcs3$ S, $3\farcs5$ W, again at position angle 139°. To cover both of these *IUE* positions, the Goldcam slit was located 9″ S. Position *c* is located 4″ N, 22″ E, at a position angle of 334°, and includes the east ansa. Position *d* is 4″ N, 8″ E at a position angle of 139°. For both of these positions, the Goldcam slit was placed 4″ N. For all four positions in NGC 7009, the overlap is reasonably good.

NGC 6720.—Position *a* is located $11\farcs2$ S, $16\farcs6$ E of the central star at position angle 124°. The Goldcam slit was placed $11\farcs2$ S, yielding reasonably good overlap. Position *b* is 16″ N, $42\farcs8$ E at position angle 295°. The Goldcam slit was $17\farcs3$ N, giving reasonably good overlap.

NGC 6210.—Both *IUE* spectra were positioned 4″ N, 8″ E at position angle $10\fdg5$. The Goldcam slit was centered 4″ N, producing fair overlap.

NGC 6826.—Position *a* is 10″ S, 10″ W of the central star at position angle 218°. Position *b* is 9″ S, 5″ E at position angle 58°. For both of these positions, the Goldcam slit was placed 9″ S, and the resulting overlap was good. Position *c* is 10″ N, 10″ E at position angle 218°. The Goldcam slit was 10″ N, with good overlap.

2.4. *Line Strengths*

Strengths of all optical and UV lines were measured using SPLOT in IRAF and are reported in Table 2. Fluxes uncorrected for reddening are presented in columns labeled $F(\lambda)$, where these flux values have been normalized to $\mathrm{H}\beta = 100$ using our observed value of $F_{\mathrm{H}\beta}$ shown in the third row from the bottom of the table. These line strengths in turn were corrected for reddening by assuming that the relative strength of $\mathrm{H}\alpha/\mathrm{H}\beta = 2.86$ and by computing the logarithmic extinction quantity c shown in the penultimate line of the table. Values for the reddening coefficients, $f(\lambda)$, are listed in the second column, where we employed Seaton's (1979) extinction curve for the UV and that of Savage & Mathis (1979) for the optical.

Because of imperfect spatial overlap between the optical and *IUE* observations for all but DDDM1, a final adjustment was made by multiplying the *IUE* line strengths by a merging factor that was determined from the theoretical ratio of either the He II lines $\lambda 1640/\lambda 4686$ or the carbon

[2] IRAF is distributed by the National Optical Astronomy Observatories, which is operated by AURA, Inc., under cooperative agreement with the National Science Foundation.

TABLE 2

UV and Optical Line Strengths

Line	$f(\lambda)$	DDDM1		IC 3568		IC 4593		NGC 7009a		NGC 7009b		NGC 7009c		NGC 7009d	
		$F(\lambda)$	$I(\lambda)$	$F(\lambda)$	$I(\lambda)$	$F(\lambda)$	$I(\lambda)$	$F(\lambda)$	$I(\lambda)$	$F(\lambda)$	$I(\lambda)$	$F(\lambda)$	$I(\lambda)$	$F(\lambda)$	$I(\lambda)$
C III λ1175	1.85	...	...	...	...	...	...	...	...	...	...	...	...	14	31
N V λ1241	1.64	...	...	...	...	...	...	3.3	5.9	5.7	12	...	...	9.5	18
C II λ1336	1.41	...	...	...	...	...	...	7.5	11	7.8	15	6.8	14	10	16
O IV] λ1402	1.31	...	...	...	...	...	...	...	...	...	...	...	...	...	...
N IV] λ1485	1.23	...	...	...	...	...	...	...	...	2.4:	4.2:	...	...	2.4	3.4
C IV λ1549	1.18	...	...	97	21	30	5.8	8.2	9.4	7.7	13	28	36	13	17
[Ne V] λ1575	1.17	...	...	...	...	...	...	...	...	1.7	2.8	73	90	2.2	2.9
He II λ1640	1.14	...	...	...	...	...	...	62	68	44	75	18	21	72	96
O III] λ1662	1.13	...	...	14	2.9	...	...	...	...	5.9	10	...	...	7.3	9.7
N III] λ1750	1.12	14	15::	...	...	...	...	3.4	3.6	4.6	7.8	8.2	9.0	9.0	12
C II λ1760	1.12	...	...	...	...	...	...	...	...	...	...	...	...	...	
Si II λ1812	1.13	...	...	...	...	...	...	...	...	...	...	...	...	1.9	2.5
Si III] λ1887	1.21	4.6	5::	...	...	...	...	...	...	...	...	...	...	...	...
C III] λ1909	1.23	7.1	8	175	40	12	2.5	51	61	53	94	58	81	64	91
[O II] λ 3727	0.29	103	105	5.2	7.0	37	42	5.5	7.5	11	12	22	41	12	15
He II + H10 λ3797	0.27	4.8	4.9	...	...	...	...	...	...	...	...	...	...	4.0	4.9
He II + H9 λ3835	0.25	6.9	7.0	...	...	...	...	...	...	...	...	...	...	...	...
[Ne III] λ3869	0.25	30	30	57	75	27	29	63	82	84	93	76	133	87	105
He I + H8 λ3889	0.25	19	19	13	17	17	19	14	18	17	18	12	20	17	21
Hϵ + [Ne III] λ3968	0.23	26	26	27	34	22	24	32	41	41	45	35	58	42	49
He II λ4026	0.21	2.0	2.1	1.6	2.0	1.8	1.9	1.9	2.3	2.2	2.4	...	...	2.1	2.4
[S II] λ4072	0.20	2.6	2.7	0.31	0.38	0.45	0.49	1.5	1.8	1.9	2.1	...	...	2.2	2.5
He II + Hδ λ4101	0.19	25	26	20	24	22	24	21	26	24	26	22	33	23	27
He II λ4198	0.16	...	...	...	...	...	...	...	...	...	...	...	...	0.21::	0.24::
C II λ4267	0.14	...	...	0.24:	0.28:	0.16:	0.17:	0.36:	0.42:	0.73	0.78	...	...	0.50	0.55
Hγ λ4340	0.13	47	48	40	46	44	47	40	45	45	47	38	50	43	47
[O III] λ4363	0.12	5.2	5.3	8.0	9.0	1.8	1.9	6.0	6.8	7.0	7.4	5.3	6.9	6.5	7.1
He I λ4471	0.09	4.8	4.9	4.4	4.8	4.7	4.9	4.7	5.2	5.2	5.4	5.5:	6.8:	4.7	5.1
He II λ4540	0.07	...	...	...	...	...	...	0.26:	0.29:	0.36	0.37	...	...	0.43	0.45
N III λ4640	0.05	...	...	1.8	1.9	2.9	2.9	4.8	5.0	5.1	5.2	...	...	4.5	4.7
He II λ4686	0.04	...	...	1.0	1.1	0.66	0.67	10	11	12	12	3.0:	3.2:	15	15
[Ar IV] λ4711 + He I λ4713	0.03	...	...	...	...	0.58	0.59	4.7	4.9	4.0	4.1	3.0	3.2	3.7	3.8
[Ar IV] λ4740	0.02	...	...	1.9	1.9	...	...	4.3	4.4	3.8	3.8	0.66::	0.69::	3.5	3.6
Hβ λ4861	0.00	100	100	100	100	100	100	100	100	100	100	100	100	100	100
He I λ4922	−0.02	1.1	1.1	...	...	1.5	1.5	1.7	1.6	1.5	1.4	2.2::	2.1::	1.4	1.4
[O III] λ4959	−0.03	148	148	370	359	182	180	399	386	402	397	442	414	404	395
[O III] λ5007	−0.04	454	453	1154	1105	565	556	1252	1198	1218	1197	1352	1234	1257	1220
[N I] λ5199	−0.09	0.44	0.44	0.01::	0.01::	...	...	...	...	0.10::	0.10::	1.2	1.0	...	...
He II λ5411	−0.13	...	...	...	...	...	...	1.2	1.0	1.1	1.0	...	...	1.3	1.2
[Cl III] λ5517	−0.16	0.21:	0.20:	.35	0.30	0.41	0.39	0.56	0.47	0.51	0.48	...	...	0.57	0.51
[Cl III] λ5537	−0.16	0.26:	0.26:	0.29	0.25	0.37	0.35	0.66	0.55	0.66	0.62	...	...	0.73	0.65

TABLE 2—*Continued*

		DDDM1		IC 3568		IC 4593		NGC 7009a		NGC 7009b		NGC 7009c		NGC 7009d	
Line	$f(\lambda)$	$F(\lambda)$	$I(\lambda)$	$F(\lambda)$	$I(\lambda)$	$F(\lambda)$	$I(\lambda)$	$F(\lambda)$	$I(\lambda)$	$F(\lambda)$	$I(\lambda)$	$F(\lambda)$	$I(\lambda)$	$F(\lambda)$	$I(\lambda)$
[N II] λ5755	−0.21	1.4	1.4	0.01::	0.01::	0.10::	0.09::	0.19	0.15	0.33	0.31	1.1::	0.71::	0.43	0.37
C IV λλ5801, 5812	−0.22	…	…	0.63	0.50	…	…	…	…	…	…	…	…	…	…
He I λ5876	−0.23	15	15	20	16	16	15	20	16	17	15	28	17	17	15
[K IV] λ6101	−0.28	…	…	…	…	…	…	0.35	0.26	…	…	…	…	0.18	0.15
He II λ6116	−0.28	…	…	…	…	…	…	…	…	…	…	…	…	…	…
[O I] λ6300	−0.31	2.4	2.3	…	…	…	…	…	…	0.28	0.24	4.4:	2.2:	0.51	0.41
[S III] λ6312	−0.31	1.8	1.7	0.44::	0.32::	0.83	0.73	1.5	1.1	1.7	1.5	…	…	2.0	1.6
[O I] λ6363	−0.32	0.85	0.84	…	…	…	…	…	…	…	…	…	…	0.23	0.18
[Ar V] λ6434	−0.34	…	…	…	…	…	…	…	…	…	…	…	…	…	…
[N II] λ6548	−0.36	18	17	…	…	3.2	2.8	2.2	1.5	5.3	4.5	…	…	7.4	5.7
Hα λ6563	−0.36	292	286	420	289	332	287	423	289	335	287	645	292	372	288
[N II] λ6584	−0.36	54	53	2.5	1.7	12	11	8.6	5.9	17	15	112	50	24	18
He I λ6678	−0.38	4.1	4.0	5.8	3.9	4.5	3.9	6.1	4.0	4.8	4.1	10	4.4	5.1	3.9
[S II] λ6716	−0.39	3.2	3.1	0.15:	0.10:	0.64	0.55	0.82	0.55	1.4	1.2	13	5.7	2.1	1.6
[S II] λ6731	−0.39	5.4	5.2	0.17:	0.11:	0.92	0.78	1.4	0.92	2.5	2.1	19	8.1	3.5	2.7
[Ar V] λ7005	−0.43	0.10	0.10	…	…	…	…	…	…	…	…	…	…	…	…
He I λ7065	−0.44	8.1	7.9	6.0	3.8	4.8	4.0	6.6	4.2	5.4	4.5	3.9	1.5	6.6	4.8
[Ar III] λ7135	−0.45	8.1	7.9	12	7.6	12	9.7	21	13	19	15	23	8.3	24	17
[Ar IV] λ7168	−0.46	0.04::	0.04::	…	…	…	…	0.25	0.15	…	…	…	…	…	…
He IIλ7178	−0.46	…	…	…	…	…	…	…	…	…	…	…	…	…	…
[Ar IV] λ7235	−0.47	…	…	…	…	…	…	0.28	0.17	0.34	0.28	…	…	0.35	0.25
He I λ7281	−0.47	0.92	0.90	1.0	0.61	…	…	0.94	0.57	0.70	0.57	…	…	0.88	0.63
[O II] λ7325	−0.48	16	16	1.2	0.74	2.9	2.4	2.5	1.5	2.4	2.0	6.6	2.3	3.1	2.2
[Cl IV] λ7529	−0.51	0.02	0.02	…	…	…	…	0.83	0.48	0.47	0.38	…	…	0.51	0.35
[Ar III] λ7751	−0.54	1.9	1.9	3.0	1.7	2.8	2.3	5.4	3.0	4.5	3.6	6.0	1.8	6.0	4.1
[Cl IV] λ8045	−0.57	…	…	…	…	…	…	2.0	1.1	1.0	0.81	1.4	0.39	1.2	0.81
He II λ8236	−0.59	…	…	…	…	…	…	0.56	0.30	0.37	0.28	…	…	0.53	0.35
P16 λ8467	−0.62	…	…	…	…	…	…	…	…	…	…	…	…	…	…
P15 λ8502	−0.62	…	…	…	…	…	…	…	…	0.56:	0.43:	…	…	0.72:	0.46:
P14 λ8544	−0.63	…	…	…	…	0.57::	0.44::	0.99:	0.51:	0.64:	0.49:	…	…	0.89:	0.57:
P13 λ8598	−0.63	…	…	…	…	0.87::	0.67::	1.1:	0.56:	0.73:	0.56:	…	…	0.99:	0.63:
P12 λ8664	−0.64	0.91::	0.88::	1.5::	0.77::	0.88::	0.68::	1.3:	0.66:	1.0:	0.78:	…	…	1.4:	0.89:
P11 λ8750	−0.64	1.1::	1.1::	1.8::	0.93::	1.2:	0.89:	2.0:	1.0:	1.2:	0.90:	3.2:	0.77:	1.8:	1.1:
P10 λ8862	−0.65	1.5:	1.4:	2.4::	1.2::	1.7:	1.3:	2.6:	1.3:	1.5:	1.2:	…	…	2.4:	1.5:
P9 λ9014	−0.67	2.0:	1.9:	3.7:	1.8:	2.0:	1.6:	2.8:	1.4:	1.8:	1.3:	…	…	2.7:	1.7:
[S III] λ9069	−0.67	21:	20:	12:	5.7:	21:	16:	43:	21:	33:	25:	73:	17:	50:	31:
P8 λ9228	−0.68	3.4:	3.3:	6.4:	3.2:	3.4:	2.6:	6.1:	3.0:	3.8:	2.8:	5.2:	1.2:	5.7:	3.5:
[S III] λ9532	−0.70	50:	48:	28:	13:	60:	45:	42:	20:	30:	22:	59:	13:	54:	33:
P7 λ9544	−0.70	4.0:	3.8:	6.1:	2.9:	6.1:	4.6:	5.2:	2.5:	3.2:	2.4:	…	…	3.8:	2.3:
log $F^{a}_{H\beta}$		−11.78		−11.40		−10.87		−10.87		−10.62		−12.15		−10.62	
c		0.023		0.45		0.18		0.46		0.19		0.95		0.31	
Merging factor[b]		1.0		0.064		0.12		0.33		1.05		0.09		0.60	

TABLE 2—*Continued*

Line	$f(\lambda)$	NGC 6720a		NGC 6720b		NGC 6210		NGC 6826a		NGC 6826b		NGC 6826c	
		$F(\lambda)$	$I(\lambda)$	$F(\lambda)$	$I(\lambda)$	$F(\lambda)$	$I(\lambda)$	$F(\lambda)$	$I(\lambda)$	$F(\lambda)$	$I(\lambda)$	$F(\lambda)$	$I(\lambda)$
C III λ1175	1.85	11	13	...	...	...	...	...	...	...	...	...	...
N V λ1241	1.64	1.4	1.5	...	...	...	...	...	...	...	...	...	...
C II λ1336	1.41	5.1	5.6	...	...	...	...	...	...	5.5:	1.5:	...	...
O IV] λ1402	1.31	5.9	6.4	...	...	...	...	...	...	...	...	...	...
N IV] λ1485	1.23	6.1	6.6	...	...	...	...	...	...	...	...	...	...
C IV λ1549	1.18	26	28	...	...	...	...	...	...	3.9:	0.97:	...	...
[Ne V] λ1575	1.17	...	...	...	...	2.4	9.1	...	...	...	...	...	...
He II λ1640	1.14	268	285	155	16	2.1	7.7	...	...	...	...	...	...
O III] λ1662	1.13	19	21	57	5.7	1.9	7.0	...	...	...	...	19::	2.7::
N III] λ1750	1.12	...	...	41	4.0	0.55	2.1	...	...	...	...	...	...
C II λ1760	1.12	...	...	...	...	...	...	...	...	7.2	1.8	...	...
Si II λ1812	1.13	...	...	...	...	...	...	...	...	...	...	...	...
Si III] λ1887	1.21	...	...	...	...	...	...	...	...	...	...	...	...
C III] λ1909	1.23	262	283	1097	121	7.6	29	70	24	78	20	120	18
[O II] λ3727	0.29	187	195	813	1093	43	45	24	24	27	29	15	19
He II + H10 λ3797	0.27	5.1	5.3	...	...	...	...	...	...	...	...	...	...
He II + H9 λ3835	0.25	6.9	7.1	...	...	...	...	...	...	...	...	4.8	6.0
[Ne III] λ3869	0.25	115	119	121	156	87	91	48	48	44	47	35	44
He I + H8 λ3889	0.25	21	22	20	26	19	20	22	22	20	21	16	19
Hϵ + [Ne III] λ3968	0.23	52	54	54	68	44	45	32	32	30	32	25	30
He II λ4026	0.21	2.2	2.3	3.4::	4.2::	2.3	2.4	2.4	2.4	2.2	2.4	1.8	2.2
[S II] λ4072	0.20	3.6	3.7	7.4:	9.1:	2.8	2.9	0.40	0.40	0.40	0.42	0.52::	0.62::
He II + Hδ λ4101	0.19	27	27	20	24	26	27	27	27	25	26	21	24
He II λ4198	0.16	0.85	0.87	...	...	...	...	...	...	...	...	...	...
C II λ4267	0.14	1.1	1.1	1.4::	1.6::	0.29	0.30	0.58	0.58	0.46	0.48	0.41:	0.46:
Hγ λ4340	0.13	48	48	41	47	48	49	48	48	47	48	41	46
[O III] λ4363	0.12	9.7	9.9	3.7:	4.2:	6.3	6.4	3.4	3.4	3.5	3.6	3.2	3.5
He I λ4471	0.09	3.9	4.0	6.6	7.3	5.3	5.4	5.2	5.2	5.2	5.3	4.8	5.1
He II λ4540	0.07	1.5	1.5	...	...	...	...	...	...	...	...	...	...
N III λ4640	0.05	2.7	2.7	...	...	...	...	1.3	1.3	1.2	1.2	...	...
He II λ4686	0.04	44	44	2.3:	2.4:	1.2	1.2	...	...	...	...	...	...
[Ar IV] λ4711 + He II λ4713	0.03	3.5	3.5	...	...	1.8	1.8	0.86	0.86	0.82	0.82	0.72:	0.73:
[Ar IV] λ4740	0.02	2.3	2.3	...	...	1.5	1.5	0.30	0.30	0.22:	0.22:	0.29::	0.29::
Hβ λ4861	0.00	100	100	100	100	100	100	100	100	100	100	100	100
He I λ4922	−0.02	0.95	0.95	...	...	1.5	1.5	1.4	1.4	1.4	1.4	1.4	1.4
[O III] λ4959	−0.03	405	403	191	185	382	380	243	243	249	247	249	243
[O III] λ5007	−0.04	1229	1222	577	553	...	...	732	732	748	739	758	732
[N I] λ5199	−0.09	1.9	1.9	26	23	...	...	...	...	0.08::	0.08::	...	...
He II λ5411	−0.13	3.7	3.6	...	...	0.07:	0.07:	...	...	...	...	...	...
[Cl III] λ5517	−0.16	1.1	1.1	...	...	0.44	0.43	0.54	0.54	0.55	0.53	0.82	0.72
[Cl III] λ5537	−0.16	0.91	0.89	...	...	0.56	0.55	0.51	0.51	0.46	0.44	0.81	0.71
[N II] λ5755	−0.21	2.8	2.7	19	15	0.62	0.60	0.09::	0.09::	0.16::	0.15::	0.15::	0.12::
C IV $\lambda\lambda$5801, 5812	−0.22	...	...	...	...	...	...	...	...	...	...	...	...

TABLE 2—*Continued*

Line	$f(\lambda)$	NGC 6720a		NGC 6720b		NGC 6210		NGC 6826a		NGC 6826b		NGC 6826c	
		$F(\lambda)$	$I(\lambda)$	$F(\lambda)$	$I(\lambda)$	$F(\lambda)$	$I(\lambda)$	$F(\lambda)$	$I(\lambda)$	$F(\lambda)$	$I(\lambda)$	$F(\lambda)$	$I(\lambda)$
He I λ5876	−0.23	11	10	23	18	16	16	15	15	16	15	18	15
[K IV] λ6101	−0.28	0.19	0.18	…	…	0.06	0.05	…	…	…	…	…	…
He II λ6116	−0.28	0.16	0.15	…	…	…	…	…	…	…	…	…	…
[O I] λ6300	−0.31	8.6	8.3	128	93	3.7	3.5	…	…	…	…	…	…
[S III] λ6312	−0.31	1.9	1.8	0.47::	0.34::	1.4	1.3	0.75	0.75	0.72	0.66	1.2	0.92
[O I] λ6363	−0.32	2.7	2.6	43	31	1.1	1.1	0.03::	0.03::	0.04	0.04	…	…
[Ar V] λ6434	−0.34	0.14	0.13	…	…	…	…	…	…	…	…	…	…
[N II] λ6548	−0.36	53	51	428	298	8.8	8.3	1.8	1.8	1.9:	1.7:	4.1	3.0
Hα λ6563	−0.36	301	286	416	289	305	287	286	286	317	287	390	288
[N II] λ6584	−0.36	168	160	1370	948	30	29	7.8	7.8	12	11	12	9.0
He I λ6678	−0.38	3.2	3.1	7.7	5.2	4.3	4.0	3.9	3.9	4.4	4.0	5.5	4.0
[S II] λ6716	−0.39	13	12	78	53	2.8	2.6	0.42	0.42	0.52	0.47	0.84	0.61
[S II] λ6731	−0.39	12	12	70	47	4.8	4.5	0.61	0.61	0.73	0.65	1.2	0.84
[Ar V] λ7006	−0.43	0.32	0.30	…	…	…	…	…	…	…	…	…	…
He I λ7065	−0.44	2.4	2.3	8.1	5.2	6.3	5.8	3.5	3.5	4.4	3.9	5.2	3.6
[Ar III] λ7135	−0.45	25	23	45	29	14	12	11	11	12	11	16	11
[Ar IV] λ7168	−0.46	0.06	0.05	…	…	…	…	…	…	…	…	…	…
He II λ7178	−0.46	0.48	0.45	…	…	…	…	…	…	…	…	…	…
[Ar IV] λ7235	−0.47	0.54	0.51	…	…	0.15	0.14	0.57	0.57	0.52	0.46	0.69	0.47
He I λ7281	−0.47	0.44	0.41	…	…	0.79	0.73	…	…	0.77	0.67	0.88	0.59
[O II] λ7325	−0.48	7.3	6.8	47	29	7.5	6.9	1.3	1.3	1.9	1.6	2.1	1.4
[Cl IV] λ7529	−0.51	0.21	0.20	…	…	0.27	0.25	…	…	…	…	…	…
[Ar III] λ7751	−0.54	5.9	5.5	13	7.2	3.3	3.0	2.4	2.5	2.9	2.5	4.1	2.6
[Cl IV] λ8045	−0.57	0.58	0.54	…	…	0.62	0.56	0.12	0.12	…	…	…	…
He II λ8236	−0.59	1.2	1.1	…	…	0.07	0.06	…	…	…	…	…	…
P16 λ8467	−0.62	0.49	0.45	…	…	0.43	0.39	…	…	0.39	0.33	…	…
P15 λ8502	−0.62	0.55:	0.50:	…	…	0.55:	0.50:	…	…	0.52:	0.44:	…	…
P14 λ8544	−0.63	0.52:	0.48:	…	…	0.65:	0.59:	0.47:	0.47:	0.58:	0.49:	1.1:	0.63:
P13 λ8598	−0.63	0.57:	0.52:	…	…	0.73:	0.66:	0.55:	0.55:	0.67:	0.56:	1.1:	0.64:
P12 λ8664	−0.64	0.83:	0.76:	…	…	1.0:	0.90:	0.78:	0.78:	0.89:	0.75:	1.3:	0.79:
P11 λ8750	−0.64	1.2:	1.1:	…	…	1.3:	1.1:	1.2:	1.2:	1.2:	0.99:	2.1:	1.2:
P10 λ8862	−0.65	1.5:	1.3:	…	…	1.5:	1.4:	1.3:	1.3:	1.5:	1.2:	2.4:	1.4:
P9 λ9014	−0.67	1.9:	1.7:	…	…	…	…	1.5:	1.5:	2.0:	1.7:	3.4:	2.0:
[S III] λ9069	−0.67	29:	26:	44:	22:	31:	28:	11:	11:	10:	8.6:	30:	17:
P8 λ9228	−0.68	3.2:	2.9:	5.3:	2.7:	4.0:	3.5:	2.8:	2.8:	3.4:	2.8:	5.4:	3.1:
[S III] λ9532	−0.70	71:	65:	101:	50:	77:	68:	39:	39:	39:	32:	105:	58:
P7 λ9544	−0.70	3.8:	3.5:	6.3::	3.1::	4.6:	4.1:	3.5:	3.5:	4.3:	3.6:	7.6:	4.2:
log $F_{H\beta}$[a]		−11.68		−12.65		−10.52		−10.96		−10.93		−11.33	
c		0.060		0.44		0.075		0.00		0.12		0.36	
Merging factor[b]		0.91		0.032		3.1		0.34		0.18		0.055	

[a] In units of ergs cm^{-2} s^{-1} in our extracted spectra.

[b] Factor by which dereddened UV line strengths are multiplied in order to merge them with optical data (see text).

lines C III] λ1909/C II λ4267. The calculation of the merging factors is described in the Appendix, and their values are listed in the last row of Table 2.

The columns headed $I(\lambda)$ list our final, corrected line strengths, again normalized to Hβ = 100. In general, intensities have uncertainties $\leq$10%; single colons indicate uncertainties up to $\sim$25%, and double colons denote doubtful detections with uncertainties up to $\geq$50%.

3. RESULTS

3.1. *Electron Temperatures and Densities*

Numerous temperature-sensitive line ratios are available in our data, enabling us to sample electron temperatures at different positions along the line of sight. For example, [O III] and [N II] temperatures, $T_{[O\ III]}$ and $T_{[N\ II]}$, are given by the intensity ratios $\lambda4363/(\lambda4959 + \lambda5007)$ and $\lambda5755/(\lambda6548 + \lambda6584)$, respectively. Two other temperatures are $T_{[O\ II]}$ and $T_{[S\ II]}$, which can be inferred from the intensity ratios of $\lambda7325/\lambda3727$ and $\lambda4072/(\lambda6716 + \lambda6731)$, respectively. In addition, the intensity ratio of $\lambda6716/\lambda6731$ is particularly sensitive to electron density, enabling the determination of the [S II] density, $N_{[S\ II]}$.

Therefore, we have computed temperatures and densities for each observed position, and the results are listed in Table 3. For each object listed in the first column, we provide the temperatures and densities in units of kelvins and cm^{-3}, respectively, determined from the above ratios. Values for $T_{[O\ III]}$ and $T_{[N\ II]}$ could be calculated in all cases. For $T_{[O\ II]}$ and $T_{[S\ II]}$, observed line ratios often implied temperatures in excess of 25,000 K, which seemed unlikely to us, and thus we do not report values in those cases. A possible cause of these excessive temperatures could be the tendency to overestimate the strengths of weak lines such as [O II] λ7325 and [S II] λ4072. Since electron temperatures vary directly with these line strengths, overestimating them would produce temperatures exceeding the actual values.

Based on our assessments of the errors in our line-strength measurements, we estimate the following uncertainties in our calculated temperatures and densities: $\delta T_{[O\ III]} = \pm 500$ K; $\delta T_{[N\ II]} = \pm 1000$ K, except for IC 3568, IC 4593, NGC 7009c, and all positions in NGC 6826, which are ± 5000 K; $\delta T_{[O\ II]} = \pm 2000$ K; $\delta T_{[S\ II]} = \pm 4000$ K; and $\delta N_{[S\ II]} = \pm 200$ cm^{-3}, except for IC 3568, which is ± 700 cm^{-3}.

We note that where multiple observations are available for different positions within a single nebula, e.g., NGC 7009, NGC 6720, and NGC 6826, values for the density or a specific temperature type are quite consistent, particularly in the case of $T_{[O\ III]}$. That the electron temperatures derived from both [O II] and [S II] lines are consistently above those determined from [O III] and [N II] is also obvious. One possible explanation is the hardening of the radiation field as it passes from the high-ionization zones nearer to the star where [O III] is found out to the lower ionization regions where [O II] and [S II] are formed. However, one would think that [N II] should share this behavior, but apparently it does not. Despite the long baselines for both [O II] and [S II] measurements, reddening errors are not to blame for the temperature discrepancy, since, in the case of [O II], the auroral lines are redward of the nebular lines, whereas in [S II], it is the nebular lines that are redder than the transauroral lines. Finally, we note again that weak line intensities tend to be overestimated, which would result in electron temperatures that are too high.

TABLE 3

ELECTRON TEMPERATURES AND DENSITIES

Object	$T_{[O\ III]}$ (K)	$T_{[N\ II]}$ (K)	$T_{[O\ II]}$ (K)	$T_{[S\ II]}$ (K)	$N_{[S\ II]}$ (cm^{-3})
DDDM1	11900	12000	...	...	3300
IC 3568	10500	6900	...	...	900
IC 4593	8200	7700	12200	...	1700
NGC 7009a	9400	12100	...	...	2900
NGC 7009b	9600	10800	...	...	3200
NGC 7009c	9300	9100	11500	...	1900
NGC 7009d	9400	10700	...	...	2900
NGC 6720a	10400	9900	12100	...	500
NGC 6720b	10200	9600	10500	12600	400
NGC 6210	9400	10900	...	...	3200
NGC 6826a	8800	8700	11100	...	1900
NGC 6826b	9000	9500	11800	...	1700
NGC 6826c	9000	8900	15200	...	1700

3.2. *Abundance Calculations*

In this project, we are concerned with the abundance ratios of He/H, O/H, C/O, N/O, and Ne/O. Paper I describes our abundance calculation method in detail. Future papers will use our newly acquired optical data to study S/O and Ar/O.

Two distinct methods exist for deriving abundances in nebulae. The first employs measured line strengths for observed ions along with knowledge of electron temperature and density to determine ionic abundances using a set of simultaneous equations. Subsequently, these ionic abundances are converted to elemental abundances by using standard correction factors to account for the unobserved ions of an element. The second method involves the calculation of a detailed photoionization model whose output line strengths match the observed ones as closely as possible. The input elemental abundances used to produce the successful model are then taken to represent the true levels in the real nebula.

Each of these methods has its own drawbacks. In the first instance, the correction factors can be sensitive to nebular properties such as matter- or radiation-boundedness. In the second case, the perennial problem is determining the uniqueness of the model solution. The number of available observational constraints can be different for each member of a sample such as ours. Thus, a systematic approach that uses only models to analyze a large number of objects suffers from nonuniformity.

For these reasons, we have developed a hybrid method in the spirit of Shields et al. (1981). The heart of the method is the use of a photoionization model to improve results from a five-level atom routine. Briefly, for each PN (or for each position within a PN where multiple positions were observed), we compile a set of merged UV and optical line strengths and use the five-level atom routine ABUN to derive an initial set of nebular abundance ratios $A^{PN}_{abun}(X)$, where X is one of the five abundance ratios listed above. We then employ the photoionization code CLOUDY, version 84 (Ferland 1990), to construct a nebular model, use ABUN to determine a set of model abundances $A^{mod}_{output}(X)$ based upon the model output line strengths, and compare these with the actual model input abundance ratios $A^{mod}_{input}(X)$. Our final set of abundance ratios $A^{PN}_{F}(X)$ for each PN (or each position within a PN) is calculated by assuming that

$$A^{PN}_{F}(X) = A^{PN}_{abun}(X)\xi(X)\ , \qquad (1)$$

where

$$\xi(X) = \frac{A^{mod}_{input}(X)}{A^{mod}_{abun}(X)}\ . \qquad (2)$$

The correction factor ξ is therefore a gauge of the accuracy of the use of the ionization correction factor method for determining abundances. The program ABUN, including the sources for atomic data, was described in detail in Paper I. Therefore, we focus on the models used to determine ξ.

3.3. *Model Results*

Photoionization models were calculated for each slit position in order to reproduce as closely as possible the physical conditions observed along the line of sight. Our models were constrained by a set of 10 important diagnostic ratios constructed directly from observed line strengths. These 10 ratios are known to describe the physical conditions of a nebula quite well. Our goal for each object (or position within an object) was to match each observed ratio to within 0.10–0.15 dex, consistent with observational uncertainties. We assumed that the central stars were blackbodies and that the nebula had a uniform density with a filling factor of unity.[3] The inner nebular radius was taken to be 0.032 pc for all models, but the outer radius was treated as a free parameter. In several cases, the best matches to the observed line strengths were produced by truncating the model inside the Strömgren radius, i.e., the model nebula was matter-bounded. Other free parameters included the stellar luminosity, nebular electron density, and nebular abundances of helium, oxygen, nitrogen, carbon, neon, and sulfur.

Table 4 summarizes our model results; for each PN (or position within a PN), we list logarithmically the observed and model-predicted values for 10 important diagnostic line ratios in the upper section of the table. The first ratio is sensitive to gas-phase metallicity and electron temperature, the second and third to the level of nebular excitation, the fourth and fifth to electron temperature and density, respectively, and the last five to abundance ratios in the order He/H, N/O, S/O, C/O, and Ne/O. The lower section of the table provides important model input parameters: the stellar effective temperature ($T_{\rm eff}$), the log of stellar luminosity log L, the electron density (N_e), and the inner and outer nebular radii (R_o and R; values of R that are less than the Strömgren distance, i.e., matter-bounded models, are indicated with a footnote). These are followed by six input abundance ratios (note that we emphasize that these abundance ratios are *not* our final abundances for each object but are the abundances necessary to produce the best model).

There are several important points about the model results that require discussion. First, we note that, with the exception of DDDM1, which is spatially unresolved, these models represent the best-fit solutions to a specific line-of-sight position within a nebula; they are *not* models of whole planetary nebulae. Model parameters were varied to match observed quantities. Thus, the stellar luminosity employed in a model may not be a dependable gauge of the true value. In the same way, the physical size of a nebula is not necessarily related directly to R_o and R. Second, the only major discrepancy between observed and predicted values in Table 4 occurs in IC 4593 for the He II/He I line ratio. Large sections of parameter space were explored in trying to render a match to this and the other ratios observed for IC 4593. We are encouraged, however, by the fact that good matches have been achieved for the nine remaining ratios, and we suggest that the lack of agreement between theory and observations for the He ratio is related to a peculiarity in the spectrum of the real central star at the He^+ ionization edge. Third, there is a discrepancy of 5 orders of magnitude in the luminosities used to model positions *a* and *b* in NGC 6720 (see Table 4). These values were required to match the greatly different ratios observed for log ($I_{\rm [O\ III]}/I_{\rm O\ III}$). It may be that position *b* is heavily shadowed and hence is characterized by much lower ionization, compared with the situation at position *a*. Finally, we note that for those PNs where more than one line-of-sight position was modeled, i.e., NGC 7009, NGC 6720, and NGC 6826, the input parameters for the individual models agree quite closely, with the major differences occurring for those parameters related to position, i.e., L and R.

Table 5 lists the correction factors ξ derived from the models, where ξ is the ratio of the input model abundance of an element to the value derived from the model-predicted line strengths using the program ABUN. A value of unity represents complete consistency between the two abundance sets. Therefore, ξ is a model-determined gauge of how closely the abundances derived with our five-level atom program agree with the actual nebular abundances. An inspection of Table 5 indicates that, with some exceptions, most frequently for N/O, values for ξ are within 20% of unity. We have employed footnotes here to indicate those models that are matter-bounded, and the large discrepancies for N/O, all greater than unity, are clearly associated with these models. Since input N/O varies little from model to model (see Table 4), the large values of ξ for N/O in these matter-bounded models must be due to the way in which [N II] λ6584 relative to [O II] λ3727 changes as one moves outward, approaching the Strömgren edge. Truncation results in a quite different line ratio than would be predicted if the model were to extend out to the Strömgren radius. This finding suggests that N/O ratios in matter-bounded nebulae generally are less secure when the standard ionization correction relation for this ratio is used.

3.4. *Derived Abundances*

Our final abundances for the seven PNs studied here are presented in Table 6 and Figure 1. Results for each position, for those PNs where more than one position was observed, are given along with averages. Abundance values in Table 6 are given on a linear scale. We point out that our final abundances in Table 6 for any one object are very consistent with the model input abundances given in Table 4 for the same object. Since the abundances in Table 6 are only indirectly connected to the model abundances in Table 4 through the use of a model-derived correction factor, this result is reassuring, albeit not altogether surprising. Our estimated uncertainties, not including systematic effects, are 15% for He/H, O/H, and Ne/O and 30%–50% for C/O and N/O. In Table 6, the last row contains solar values for the corresponding ratios taken from Grevesse & Anders (1989) for comparison, while the last column lists the Peimbert class of each object. Figure 1 shows our abundance ratios in logarithmic form and normalized to solar values, where averages have been plotted for those PNs in which more than one position was observed. Ratios derived in this paper are shown with filled symbols, using symbol shape to represent specific objects as defined in the figure caption. For comparison, abundance ratios taken from the literature (see the figure caption for sources) are shown with open

[3] While most PNs are known to have filling factors significantly less than unity, the only measurable quantity affected by the filling factor is the nebular luminosity, a parameter we are not using to constrain our models. Thus, using the same filling factor for all of the nebulae influences our abundance results in no significant way.

TABLE 4

A. Observations and Models

	DDDM1		IC 3568		IC 4593		NGC 7009a		NGC 7009b		NGC 7009c		NGC 7009d	
Ratio	Obs.	Model	Obs.	Model	Obs.	Model	Obs.	Model	Obs.	Model	Obs.	Model	Obs.	Model
log $[(I_{[O\ II]} + I_{[O\ III]})/H\beta]$	0.86	0.78	1.18	1.27	0.90	1.08	1.21	1.25	1.21	1.16	1.23	1.15	1.22	1.12
log $I_{[O\ II]}/I_{[O\ III]}$	−0.77	−0.76	−2.33	−2.35	−1.25	−1.24	−2.33	−2.33	−2.12	−2.19	−1.60	−1.56	−2.03	−2.02
log $I_{He\ II/He\ I}$	...	−2.78	−1.16	−1.21	−1.34	−2.06	−0.17	−0.25	−0.12	−0.21	−0.71	−0.56	−0.0064	0.08
log $(I_{\lambda 4363}/I_{\lambda 5007})$	−1.93	−1.97	−2.09	−1.93	−2.47	−2.45	−2.25	−2.08	−2.21	−2.17	−2.25	−2.19	−2.23	−2.21
log $(I_{\lambda 6716}/I_{\lambda 6731})$	−0.23	−0.23	−0.053	−0.074	−0.15	−0.03	−0.23	−0.22	−0.24	−0.22	−0.15	−0.22	−0.23	−0.22
log $I_{He\ I/H\beta}$	−0.82	−0.85	−0.80	−0.77	−0.83	−0.77	−0.81	−0.75	−0.82	−0.76	−0.78	−0.74	−0.83	−0.79
log $I_{6584/3727}$	−0.29	−0.28	−0.61	−0.58	−0.60	−0.53	−0.11	−0.15	0.079	−0.016	0.08	0.09	0.08	0.05
log $I_{6724/3727}$	−1.10	−1.04	−1.52	−1.51	−1.51	−1.55	−0.71	−0.79	−0.56	−0.59	−0.48	−0.47	−0.56	−0.47
log $I_{1909/5007}$	−1.75	−1.67	−1.44	−1.50	−2.35	−2.31	−1.29	−1.34	−1.10	−1.08	−1.18	−1.06	−1.13	−1.05
log $I_{3869/5007}$	−1.17	−1.13	−1.17	−1.21	−1.28	−1.31	−1.16	−1.11	−1.11	−1.12	−0.97	−0.94	−1.07	−1.05

B. Model Input Parameters

Parameter	DDDM1	IC 3568	IC 4593	NGC 7009a	NGC 7009b	NGC 7009c	NGC 7009d
T_{eff} (10^3 K)	40	41	40	77	77	77	77
log $L/L_\odot$	5.81	9.84	7.36	4.99	4.24	4.24	3.34
N_e	4000	1000	600	3200	3200	3200	3200
R_o (pc)	0.032	0.032	0.032	0.032	0.032	0.032	0.032
R (pc)	0.35	4.9[a]	1.8[a]	0.17[a]	0.10[a]	0.13[a]	0.047[a]
He/H	0.096	0.11	0.11	0.13	0.13	0.13	0.13
O/H ($\times 10^4$)	1.07	2.57	6.46	4.27	4.27	4.27	4.27
C/O	0.063	0.15	0.085	0.43	0.85	0.78	1.58
N/O	0.30	0.40	0.26	0.46	0.52	0.52	0.52
Ne/O	0.14	0.11	0.12	0.14	0.14	0.22	0.17
S/O	0.057	0.038	0.014	0.038	0.048	0.048	0.048

TABLE 4—*Continued*

A. Observations and Models

Ratio	NGC 6720a		NGC 6720b		NGC 6210		NGC 6826a		NGC 6826b		NGC 6826c	
	Obs.	Model	Obs.	Model	Obs.	Model	Obs.	Model	Obs.	Model	Obs.	Model
log $[(I_{[O\,II]} + I_{[O\,III]})/H\beta]$	1.27	1.41	1.26	1.26	1.18	1.08	1.00	1.09	1.00	1.09	1.00	1.07
log $(I_{[O\,II]}/I_{[O\,III]})$	−0.93	−0.93	0.17	0.21	−1.51	−1.51	−1.63	−1.61	−1.63	−1.61	−1.71	−1.60
log $I_{He\,II/He\,I}$	0.62	0.61	−0.87	0.23	−1.12	−1.21	...	−1.54	...	−1.54	...	−1.55
log $(I_{\lambda4363}/I_{\lambda5007})$	−2.09	−2.01	−2.12	−2.18	−2.23	−2.17	−2.33	−2.28	−2.33	−2.28	−2.32	−2.30
log $(I_{\lambda6716}/I_{\lambda6731})$	0.014	0.025	−0.049	0.047	−0.24	−0.28	−0.16	−0.17	−0.16	−0.17	−0.14	−0.17
log $I_{He\,I/H\beta}$	−0.98	−0.94	−0.75	−0.77	−0.81	−0.76	−0.83	−0.78	−0.83	−0.78	−0.82	−0.78
log $I_{6584/3727}$	−0.086	−0.051	−0.062	−0.021	−0.20	−0.11	−0.48	−0.39	−0.48	−0.39	−0.33	−0.38
log $I_{6724/3727}$	−0.92	−0.88	−1.04	−0.99	−0.80	−0.88	−1.35	−1.33	−1.35	−1.33	−1.13	−1.17
log $I_{1909/5007}$	−0.64	−0.57	−0.66	−0.58	−1.58	−1.50	−1.52	−1.50	−1.52	−1.50	−1.61	−1.53
log $I_{3869/5007}$	−1.01	−0.96	−0.55	−0.51	−1.08	−0.98	−1.19	−1.16	−1.19	−1.16	−1.22	−1.16

B. Model Input Parameters

Parameter	NGC 6720a	NGC 6720b	NGC 6210	NGC 6826a	NGC 6826b	NGC 6826c
T_{eff} (10^3 K)	150	150	60	50	50	50
log $L/L_\odot$	5.33	1.12	4.11	5.27	5.27	5.27
N_e	500	500	6300	1900	1900	1900
R_o (pc)	0.032	0.032	0.032	0.032	0.032	0.032
R (pc)	0.87	0.072	0.076[a]	0.28[a]	0.28[a]	0.28[a]
He/H	0.12	0.12	0.12	0.11	0.11	0.11
O/H ($\times 10^4$)	7.23	6.76	3.39	4.27	4.27	4.27
C/O	1.20	1.02	0.23	0.34	0.34	0.34
N/O	0.39	0.35	0.32	0.26	0.26	0.26
Ne/O	0.18	0.18	0.20	0.14	0.14	0.14
S/O	0.011	0.01	0.029	0.013	0.013	0.019

[a] Matter-bounded models.

TABLE 5

CORRECTION FACTORS (ξ)

Object	He/H	O/H	C/O	N/O	Ne/O
DDDM1	0.98	0.89	0.74	1.32	0.91
IC 3568[a]	0.89	0.82	1.40	2.76	0.88
IC4593[a]	0.88	0.94	0.95	2.58	0.87
NGC 7009a[a]	0.90	0.91	1.57	1.69	0.84
NGC 7009b[a]	0.93	0.90	1.30	1.61	0.83
NGC 7009c[a]	0.91	0.89	1.03	1.28	0.81
NGC 7009d[a]	0.92	0.83	1.05	1.50	0.81
NGC 6720a	0.92	0.88	0.97	0.83	0.78
NGC 6720b	0.76	0.82	0.49	0.84	0.25
NGC 6210[a]	0.91	0.89	0.91	1.45	0.82
NGC 6826a[a]	0.90	0.88	0.97	1.88	0.84
NGC 6826b[a]	0.90	0.88	0.97	1.88	0.84
NGC 6826c[a]	0.90	0.88	0.97	1.87	0.84

[a] Matter-bounded models.

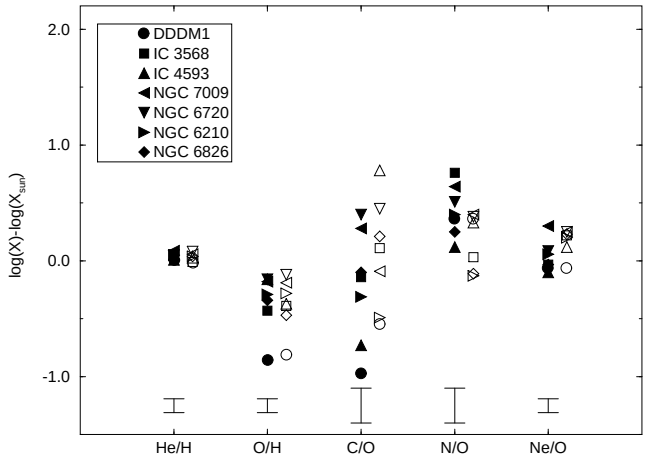

FIG. 1.—The five abundance ratios computed here and normalized to their solar values (Grevesse & Anders 1989) are plotted logarithmically. The symbol shapes are used to designate each object. The filled symbols are our results, while the open symbols refer to results from other studies found in the literature: values for IC 4593 were taken from Bohigas & Olguín (1996), C/O for DDDM1 is from Howard, Henry, & McCartney (1997), and, consistent with the upper limit given in Clegg, Peimbert, & Torres-Peimbert (1987), all other C/O values are from Rola & Stasińska (1994; their ratios as derived from C III] λ1909); all remaining abundance ratios are from Perinotto (1991).

symbols. Representative error bars are given for each abundance ratio to show uncertainties.

Note that our results for He/H, O/H, and Ne/O are very consistent with earlier measurements. All seven PNs have subsolar O/H, with the halo object DDDM1 being the most metal poor, as expected. In addition, Ne/O is close to solar in all objects, consistent with the idea that both of these elements are produced by stars of similar mass.

In the cases of C/O and N/O, we see a large spread among our seven objects. Note that all objects have N/O above solar. In addition, C/O is markedly below solar in DDDM1 and IC 4593 but well above solar in NGC 6720 and NGC 7009. In the case of IC 4593, our derived value of C/O is roughly 20 times smaller than the ones published by Bohigas & Olguín (1996) and French (1983), both of whom used optical recombination lines of carbon in their analysis. Bohigas & Olguín derived their carbon abundance for IC 4593 using the C III λ4648 line, which is often blended with [O II] λ4649, while French used both C III λ4648 and (uncertain) C II λ4267 to derive carbon abundances. We note that our C/O value for IC 4593 as estimated from C II λ4267 in Table 7 is consistent with our results from the C III] λ1909 line. Finally, our derived N/O values are higher for most objects, the result of using values for ξ that are significantly larger than unity.

A straightforward determination of carbon abundances is hindered by the long-standing problem whereby abundances inferred from the C II λ4267 recombination line are consistently several times greater than values determined from the collisionally excited line C III] λ1909 (see Rola & Stasińska 1994 for a recent discussion of this problem). Since we were able to measure λ4267 in our data at most observed locations, we have estimated C/O ratios implied by this line, employing the data for the relevant effective recombination coefficient given in Péquinot, Petitjean, & Boisson (1991). Results of this exercise are shown in Table 7, where, for each position listed in the first column, we give $N(C^{+2})_{\lambda 4267}/N(C^{+2})_{\lambda 1909}$, the predicted ratio of the number density of C^{+2}, in the second column. Then, since $C/O \approx C^{+2}/O^{+2}$ (Rola & Stasińska 1994; Paper I), we scaled the C/O ratios in Table 6 derived from the λ1909 line by multiplying them by the values in the second column of Table 7 to arrive at the estimates of recombination C/O reported in the third column. We give results for each observed position along with an unweighted average for

TABLE 6

DERIVED ABUNDANCES

Object	He/H	O/H ($\times 10^{-4}$)	C/O	N/O	Ne/O	Type
DDDM1	0.10	1.17	0.046	0.30	0.12	Halo
IC 3568	0.11	3.14	0.31	0.75	0.13	II–III
IC 4593	0.10	5.95	0.080	0.17	0.11	III
NGC 7009a	0.11	5.76	0.81	0.50	0.14	
NGC 7009b	0.12	5.34	0.94	0.66	0.15	
NGC 7009c	0.12	5.82	0.70	0.52	0.21	
NGC 7009d	0.11	5.46	0.77	0.61	0.17	
NGC 7009 (average)	0.12	5.60	0.81	0.57	0.28	II–III
NGC 6720a	0.11	6.35	1.47	0.49	0.17	
NGC 6720b	0.11	5.52	0.71	0.35	0.16	
NGC 6720 (average)	0.11	5.94	1.09	0.42	0.17	II–III
NGC 6210	0.11	4.40	0.21	0.33	0.16	II–III
NGC 6826a	0.10	3.97	0.38	0.19	0.14	
NGC 6826b	0.10	3.86	0.32	0.23	0.13	
NGC 6826c	0.10	3.81	0.31	0.28	0.13	
NGC 6826 (average)	0.10	3.88	0.34	0.23	0.13	II–III
Sun[a]	0.098	8.51	0.43	0.13	0.14	

[a] Grevesse & Anders 1989.

TABLE 7

C/O FROM RECOMBINATION

Object	$\frac{N(C^{+2})_{\lambda 4267}}{N(C^{+2})_{\lambda 1909}}$	C/O
DDDM1	...	...
IC 3568	3.27	1.01
IC 4593	3.12	0.25
NGC 7009a	1.29	1.04
NGC 7009b	1.90	1.79
NGC 7009c	...	...
NGC 7009d	1.21	0.93
NGC 7009 (average)		1.25
NGC 6720a	1.84	2.70
NGC 6720b	5.15	3.66
NGC 6720 (average)		3.18
NGC 6210	2.65	0.56
NGC 6826a	2.87	1.09
NGC 6826b	3.17	1.01
NGC 6826c	3.27	1.01
NGC 6826 (average)		1.04

those PNs in which we obtained data at more than one location. The numbers in the second column provide a good comparison of the recombination and collisional excitation methods for inferring C/O. As seen in many previous studies, the recombination method consistently implies a significantly larger value for C/O. However, because of the uniformly weak strength of C II λ4267, we have adopted the C/O abundances determined from the C III] λ1909 line for the *final* values in our study for this abundance ratio.

A discussion of the implications for stellar nucleosynthesis is postponed until abundances for our entire sample have been determined.

4. SUMMARY

This paper is the third in a series reporting on a study of carbon and other abundances in a well-defined sample of planetary nebulae representing a broad range in progenitor mass and metallicity. We have obtained new optical spectra from 3700 to 9600 Å at specific positions in our program objects in order to overlap spatially as nearly as possible with earlier *IUE* sites. We make use of the Final Archive database of the *IUE* spectra, in which the data have been reduced under a new, consistent system of algorithms. We have measured collisionally excited emission lines of carbon and coupled these measurements to our new optical line strengths to determine abundance ratios of He/H, O/H, C/O, N/O, and Ne/O for seven PNs: DDDM1, IC 3568, IC 4593, NGC 6210, NGC 6720, NGC 6826, and NGC 7009. *IUE* and optical spectra for the same line-of-sight position were merged using the ratio He II λ1640/λ4686, or the C III] λ1909/C II λ4267 ratio when both He II lines were unavailable. In those positions where both the helium and carbon lines were measurable, we found reasonable consistency between these two methods. To our knowledge, this is the first attempt to use the carbon line ratio for merging UV and optical spectra.

Electron temperatures and densities were determined at all locations. Derived values for different positions within the same nebula were found to be quite consistent.

Nebular abundances were inferred by using a hybrid method that couples an empirical five-level atom calculation with a photoionization model that is used to fine-tune the ionization correction factor. Thus, a photoionization model was produced for each object in which 10 important diagnostic line ratios were matched satisfactorily. Many of the models for our objects were matter-bounded and, as a result, produced a large abundance correction factor for N/O in particular. This finding implies that the standard ionization correction factors for the N/O ratio are unsatisfactory when the nebula is optically thin.

Our abundance results show a wide spread in C/O and N/O ratios among the objects, while He/H, O/H, and Ne/O ranges are much narrower, all of which is consistent with previous studies. In those PNs where more than one line-of-sight position was observed, derived properties were consistent among those positions, thus adding credence to our results and especially our abundance-determining techniques. While our final C/O abundance ratios were determined using collisionally excited lines, we also estimated values for this ratio using the recombination line C II λ4267. Consistently, we found that ratios produced by the latter method are several times greater than those produced by the former, as reported in many studies in the literature.

This project is supported by NASA grant NAG 5-2389. K. B. K. also acknowledges support from a Cottrell College Science grant of Research Corporation, from a Keck Foundation grant to the Keck Northeast Astronomy Consortium (KNAC), and from the Williams College Bronfman Science Center and the Dean of Faculty Office. R. B. C. H. is grateful to the University of Oklahoma for support of travel to KPNO. We thank Cathy Imhoff, Walter Feibelman, and Fred Bruhweiler for help in tracking down *IUE* positional information. We thank Jackie Milingo (OU) and Tim McConnochie (Williams College 1998) for their assistance with the observations. We are grateful to KPNO for funding McConnochie's observing trip. We also thank the ever helpful KPNO staff, especially Ed Carder and Jim De Veny.

APPENDIX

DETERMINATION OF THE MERGING FACTOR

The optical and *IUE* observations were made using slits of different sizes. Due to this, as well as to inherent differences in the two instruments and data-reduction algorithms, one needs to determine a merging factor at each location, i.e., a number by which the UV line strengths are multiplied in order to correct for a systematic offset in the two flux-calibrated spectra for each nebular location.

Calculating a merging factor requires that we know both the observed and theoretical values of a ratio involving two emission lines, one appearing in the UV and the other in the optical, but produced by the same ion. The merging factor is obtained by dividing the theoretical by the observed ratio.

Two such ratios are He II λ1640/He II λ4686 and C III] λ1909/C II λ4267. We measured the values of one or both of these ratios in all of our target positions. The theoretical values for the He line ratio were determined using recombination results in Storey & Hummer (1995) along with necessary electron temperatures and densities inferred from our optical observations. The theoretical carbon line ratios were determined using the empirical fit in Kaler (1986). Because of the dependence of the C III]/C II ratio on the generally weak C II λ4267 recombination line as well as the temperature-sensitive collisionally

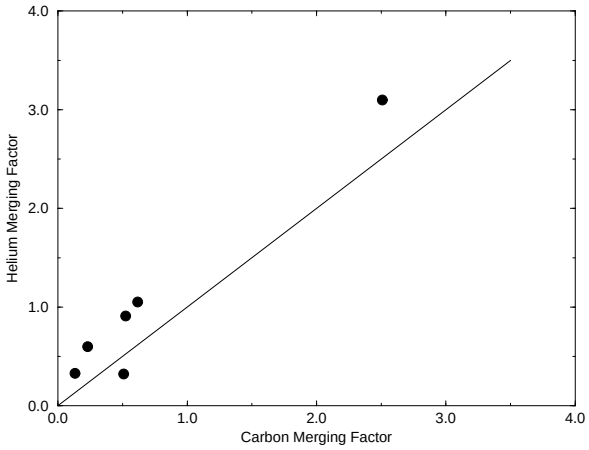

FIG. 2.—Helium merging factor vs. carbon merging factor for those nebular positions for which both could be measured. The solid line shows the locus of one-to-one correspondence.

excited C III] λ1909 line, the temperature-insensitive He ratio was preferred for determining the merging factor. Thus, when joining UV and optical spectra, the carbon ratio was employed only in those cases when He II λ1640 was not observed. Merging factors for NGC 7009, NGC 6720, and NGC 6210 were computed from the helium lines, while for IC 3568, IC 4593, and NGC 6826 the carbon lines were employed.

We note that for those objects for which both ratios were available, we found good consistency between the two factors. This is shown in Figure 2, where we plot the merging factor determined from the helium lines versus that from the carbon lines for those nebular positions where both factors could be calculated. The solid line shows where points would lie if factors at each location were equal. Clearly, the He factor tends to be systematically larger than the C factor, but for reasons that are not obvious. It is possible that this offset is related to the tendency to overestimate the strength of a weak line such as C II λ4267. However, there is good evidence here overall for rough agreement in merging factors, a result that supports the use of each of these factors. We believe that this is the first time that the carbon lines have been used in this manner to combine UV and optical spectra.

The merging factor used to scale data at each location is given in the last row of Table 2. If the *IUE* and Goldcam slits had overlapped perfectly, then the value of the merging factor should be unity, ignoring instrumental effects. Since the ratio of slit areas was 1:2 (Goldcam:*IUE*), then we would expect merging factors to fall within roughly a factor of 2 of unity. However, the results in Table 2 show that this number is below 0.3 for six of our 13 positions measured. In attempting to understand the cause of these low merging factors, we considered such things as the quality of slit overlap, as discussed in § 2.3, the particular line ratio used to determine the merging factor, the excitation level of the object, the electron density, and whether or not the position appears to be matter-bounded. For example, although we believe that the slit overlap for IC 3568 is good, the merging factor is unexpectedly low. Likewise, the quality of slit position matchup for the other five positions with merging factors below 0.3 is "reasonably good." In addition, for four of the six positions in question, the merging factor was determined using the carbon ratio; thus, it is not obvious that the technique used to determine the merging factor is itself at fault. Using the [O II]/[O III] line ratio as an indicator of excitation, we find no clear excitation difference between the six positions with low merging factors and those with values closer to unity. Nor does any pattern emerge when either electron density or the question of matter-boundedness is considered. Curiously, however, all of the merging factors differing significantly from unity are also *less than* unity, indicating that fluxes measured with the *IUE* are consistently too large with respect to the optical fluxes, even after accounting for the factor of 2 difference in slit area. While this might be indicative of calibration problems with one of the instruments, we would also expect the effect to appear at all other positions as well, which is not the case.

Alas, there appears to be no obvious connection between these properties and the calculated merging factor, and thus we are forced to conclude that, while in most instances the slit overlap appears to have been good, the smaller area of the Goldcam slit may have frequently sampled regions with lower surface brightness, perhaps by excluding knots present in the *IUE* slit. However, we argue that, given the apparent consistency between the He and C merging factors shown in Figure 2, their use in joining the UV and optical spectra for the current objects is justified and is no doubt better than applying no correction at all.

We plan to pursue the question of merging factors using a larger database in a future paper.

REFERENCES

Acker, A., Ochsenbein, F., Stenholm, B., Tylenda, R., Marcout, J., & Schohn, C. 1992, The Strasbourg-ESO Catalogue of Galactic Planetary Nebulae (Garching: ESO)
Bohigas, J., & Olguín, L. 1996, Rev. Mexicana Astron. Astrofis., 32, 47
Clegg, R. E. S., Peimbert, M., & Torres-Peimbert, S. 1987, MNRAS, 224, 761
Ferland, G. J. 1990, Ohio State Univ. Rep. 90-02
French, H. B. 1983, ApJ, 273, 214
Grevesse, N., & Anders, E. 1989, in AIP Conf. Proc. 183, Cosmic Abundances of Matter, ed. C. J. Waddington (New York: AIP), 1
Henry, R. B. C., Kwitter, K. B., & Buell, J. 1998, Rev. Mexicana Astron. Astrofis., in press
Henry, R. B. C., Kwitter, K. B., & Howard, J. W. 1996, ApJ, 458, 215 (Paper I)
Howard, J. W., Henry, R. B. C., & McCartney, S. 1997, MNRAS, 284, 465
Kaler, J. B. 1986, ApJ, 308, 337
Kwitter, K. B., & Henry, R. B. C. 1996, ApJ, 473, 304 (Paper II)
Péquignot, D., Petitjean, P., & Boisson, C. 1991, A&A, 251, 680
Perinotto, M. 1991, ApJS, 76, 687
Rola, C., & Stasińska, G. 1994, A&A, 282, 199
Savage, B. D., & Mathis, J. S. 1979, ARA&A, 17, 73
Seaton, M. J. 1979, MNRAS, 187, 73P
Shields, G., Aller, L. H., Keyes, C. D., & Czyzak, S. J. 1981, ApJ, 248, 569
Storey, P. J., & Hummer, D. G. 1995, MNRAS, 272, 41